2008 American Control Conference
Westin Seattle Hotel, Seattle, Washington, USA
June 11-13, 2008

An Improved Version of the RBode Plot

Lu Xia, William Messner

Abstract— **This paper presents an improved version of the Robust Bode (RBode) plot, in which a robust performance criterion is explicitly translated into allowable and forbidden regions on the open-loop Bode plot of a compensated SISO system. With the RBode plot robust controllers can be directly synthesized with classical loop shaping. The design concept is to shape the open-loop response to avoid entering the forbidden regions on magnitude and phase subplots defined by the boundary functions. The paper provides a clearer derivation of the RBode plot and emphasizes the fact that the weighting functions of the robust performance criterion need not be transfer functions. The improved RBode plot is applied to the design of the controller for an Lateral Tape Motion compensation system.**

I. INTRODUCTION

One difficulty with the loop shaping technique for designing controllers is that the closed-loop specifications often translate only to rather general specifications on the open-loop frequency response such as high gain at low frequencies for good reference tracking and disturbance rejection, and low gain at high frequencies for good noise rejection. Typically robustness specifications are limited to lower bounds on the gain margin and phase margin, which do not account for the specific features of the plant characteristics such as uncertainties in dynamics or nonlinearities. The closed-loop performance specifications are hardest to translate to open-loop characteristics near the open-loop 0 dB crossover, because of the complicated relationship between the open-loop gain and phase and the closed-loop gain when the open-loop gain is approximately unity.

Other tools are widely used for analyzing or synthesizing controllers to meet more detailed robustness specifications. H_∞ and μ-synthesis, for example, are automated methods for designing controllers to achieve robust performance in the presence of plant uncertainties [1][2]. However, these automated tools often do not provide much insight into the relationship between the open loop frequency response and the performance. Also these tools require that uncertainties and performance specifications are described by transfer functions, which sometimes are hard to construct and may result in conservative designs.

This paper presents an improved version of the the Robust Bode plot (RBode plot), which was originally introduced in [3]. In RBode plots, boundary functions partition the conventional Bode plots into regions that do and do not meet specific robust performance criteria. Figure 11 shows two examples of RBode plots in which the robust performance is violated, while Figure 12 shows an example of an RBode plot in which the system satisfies the robust performance criterion. In contrast to the earlier version of the RBode plot, the forbidden regions are explicitly designated by cross hatching. An important aspect of these RBode plots is that the uncertainty weighting function used to construct the plot is not a transfer function.

The RBode plots can help the designer achieve desired closed-loop performance specifications by showing on the open-loop Bode plot how a particular frequency response feature relates to the robustness characteristics. The strategy for compensator design with loop shaping with the RBode plot is to shape the open-loop response to assure that no intersections occur between boundary functions and the open-loop frequency response at any frequency.

The paper is organized as follows: Section II presents a new derivation the RBode plot boundary functions which includes plots illustrating how the boundary functions of the forbidden region of the magnitude plot are derived from a quadratic inequality and how teh boundary functions are derived from a trigonometric inequality. Section III shows a design example for active tape steering control system using RBode plot using weighting function that is not a transfer function. Concluding remarks appear in Section IV.

II. DERIVATION OF RBODE PLOTS

In RBode plots, boundary functions which represent performance bounds are added to the open-loop magnitude and phase plots to partition the conventional Bode plots into regions that do and do not meet specific robust performance criteria. This sections gives the derivation of the RBode boundary functions.

A. The Robust Performance Criterion

Consider the uncertain plant described by multiplicative uncertainty model shown in Figure 1, where $\tilde{P}(s)$ is the uncertain plant, and $P(s)$ is a known transfer function representing the nominal plant. The uncertainty model, $\Delta(s)$, is an unknown but stable transfer function with $|\Delta(j\omega)| <$

This research is supported by Imation Corporation and NIST MTS funding.

The authors are with the Data Storage Systems Center, Carnegie Mellon University, Pittsburgh, PA 15213 lxia,bmessner@andrew.cmu.edu

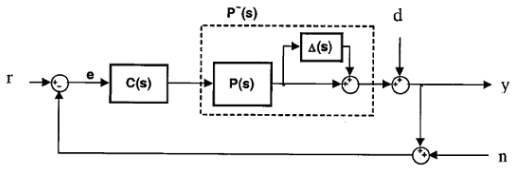

Fig. 1. Block diagram with multiplicative model uncertainty.

.

$|W_u(\omega)|$, for all ω. The weighting function, $W_u(\omega)$ satisfies

$$\left|\frac{\tilde{P}(\jmath\omega)}{P(\jmath\omega)} - 1\right| \leq |W_u(\omega)|, \text{ for all } \omega, \tag{1}$$

where the magnitude response of $W_u(\omega)$ is an upper bound of the magnitude of the model uncertainty, $|\Delta(\omega)|$.

The desired performance of the system is specified by a weighting function $W_s(\omega)$ such that

$$|\tilde{S}(\jmath\omega)| < |W_s(\omega)|^{-1}, \text{ for all } \omega, \text{ where } \tilde{S}(s) \equiv \frac{1}{1+\tilde{P}(s)C(s)} \tag{2}$$

If the nominal loop transfer function $L(s) \equiv P(s)C(s)$ is stable, a necessary and sufficient condition for a SISO controller to achieve robust performance is [4]

$$|W_u(\omega)T(\jmath\omega)|+|W_s(\omega)S(\jmath\omega)| = \frac{|W_u(\omega)L(\jmath\omega)| + |W_s(\omega)|}{|1+L(\jmath\omega)|} < 1 \tag{3}$$

for all frequencies ω.

B. Derivation of the RBode Phase boundary functions

The derivation of the phase boundary functions for the RBode plot is easier than the derivation for the magnitude boundary functions. Using the fact that $L = |L|cos\,(arg(L)) + j|L|sin\,(arg(L))$, the necessary and sufficient condition that closed-loop achieves robust performance given by inequality (3) is equivalent to the requirement that

$$\frac{|W_u|^2|L|^2 + 2|W_u||W_s||L| + |W_s|^2}{1 + 2|L|\cos(\arg(L)) + |L|^2} < 1. \tag{4}$$

for all frequencies ω where $\jmath\omega$ has been suppressed for notational convenience. Solving (4) for $\cos(\arg(L))$ transforms the robust performance criterion to

$$\cos(\arg(L)) > \frac{|W_s|^2 - 1 + 2|W_sW_u||L| + (|W_u|^2-1)|L|^2}{2|L|}. \tag{5}$$

for all frequencies ω.

The phase boundary functions define the regions for which inequality (5) holds. The principal value of the phase boundary between 0 and 180° is (Figure 2)

$$\phi_R \equiv \arccos\left(\frac{|W_s|^2 - 1 + 2|W_sW_u||L| + (|W_u|^2-1)|L|^2}{2|L|}\right). \tag{6}$$

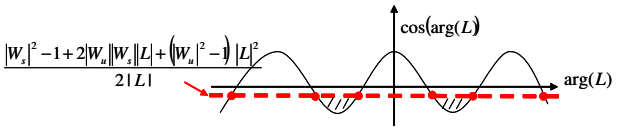

Fig. 2. Illustrations of arccos for RBode phase boundary function derivation.

The principal value is only defined when the argument to the right hand side is between -1 and 1. The upper and lower boundaries are

$$\begin{aligned} \phi_{Rk_u} &\equiv 360^\circ k + \phi_R \text{ and,} \\ \phi_{Rk_l} &\equiv 360^\circ k - \phi_R, \\ \text{for} &\quad k = \cdots, -2, -1, 0, 1, 2, \cdots \end{aligned}$$

The feedback system will satisfy the robust performance criterion (5) and equivalently the robust performance criterion (3), if for each frequency ω, either the argument of the right hand side of (6) is less than -1, or the open-loop phase, $\arg(L)$ lies between ϕ_{Rk_l} and ϕ_{Rk_u} for some k.

Plotting the functions ϕ_{Rk_l} and ϕ_{Rk_u} and the open-loop Bode phase chart on the same axes generates the phase chart of the RBode plot. Any intersection between the graphs of ϕ_{Rk_l} and ϕ_{Rk_u} and the open-loop phase response indicates that the system does not achieve robust performance.

C. Derivation of the RBode Magnitude boundary functions

The derivation of the magnitude boundary functions employs the relation (4), but is much more complicated than the derivation of the phase boundary functions. Squaring both sides of (4), and bringing all functions to the left hand side results in

$$(1-|W_u|^2)|L|^2 + 2(\cos(\arg(L)) - |W_u||W_s|)|L| + 1 - |W_s|^2 > 0. \tag{7}$$

The open-loop magnitude $|L|$ can satisfy inequality (7) depending on the sign of the lead coefficient $1-|W_u|^2$ and the nature of the roots of the quadratic equation

$$\begin{aligned} A(\lambda) &\equiv (1-|W_u|^2)\lambda^2 + \\ &\quad 2(\cos(\arg(L)) - |W_u||W_s|)\lambda + 1 - |W_s|^2 \\ &\quad = 0. \end{aligned} \tag{8}$$

For $1-|W_u|^2 \neq 0$ define the roots of (8) as

$$\begin{aligned} \lambda_1 &\equiv \frac{|W_u||W_s| - \cos(\arg(L)) - \sqrt{D}}{1-|W_u|^2} \\ \lambda_2 &\equiv \frac{|W_u||W_s| - \cos(\arg(L)) + \sqrt{D}}{1-|W_u|^2}, \end{aligned}$$

where

$$\begin{aligned} D \equiv (\cos(\arg(L)) - |W_u||W_s|)^2 - \\ (1-|W_u|^2)(1-|W_s|^2) \end{aligned} \tag{9}$$

For $1-|W_u|^2 = 0$ define the root of (8) as

$$\lambda_1 \equiv \frac{|W_s|^2 - 1}{2(\cos(\arg(L) - |W_uW_s|)}. \tag{10}$$

Note that the roots are functions of $\jmath\omega$.

Determining the magnitude contour functions requires considering several cases corresponding to the different combinations of the roots and the coefficients of equation (8). These cases provide some insight into the selection of W_u and W_s. Each case leads logically to the definition of an upper boundary function M_{Ru} and a lower boundary function M_{Rl} such that the system satisfies the robust performance criterion if and only if

1) At all frequencies where $M_{Ru} > M_{Rl}$ the graph of $|L|$ lies between M_{Ru} and M_{Rl};
2) At all frequencies where $M_{Ru} < M_{Rl}$ the graph of $|L|$ lies either below M_{Ru} or above M_{Rl}; and
3) There are no frequencies at which neither M_{Ru} nor M_{Rl} exist.

Two useful facts about the roots of equation (8) for the derivations of the contour functions are

$$\lambda_1 + \lambda_2 = 2\frac{\cos(\arg(L)) - |W_u||W_s|}{|W_u|^2 - 1}, \qquad (11)$$

and

$$\lambda_1\lambda_2 = \frac{1 - |W_s|^2}{1 - |W_u|^2}. \qquad (12)$$

There are five main cases depending on the magnitude of $|W_u|$ and $|W_s|$ relative to unity.

1) Frequencies where $|W_u| < 1$ and $|W_s| \leq 1$. These are the frequencies where the magnitude of the modeling uncertainty is less than the magnitude of the nominal model itself (i.e. there is relatively high confidence in the model), and disturbance rejection is not required.

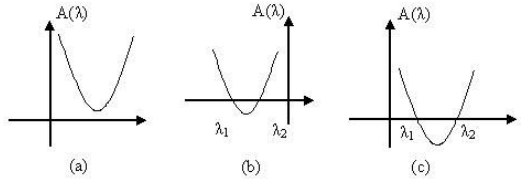

Fig. 3. Illustrations of $A(\lambda)$ for the three cases when $|W_u| < 1$ and $|W_s| \leq 1$.

   a) If $D < 0$, then λ_1 and λ_2 are both complex, and any positive value of $|L|$ satisfies the inequality (7). Therefore define $M_{Ru} \equiv \infty$ and $M_{Rl} \equiv 0$ (Figure 3(a)).
   b) If $D \geq 0$ and $\cos(\arg(L)) - |W_u||W_s| \geq 0$, then it follows from (11) that $\lambda_1 + \lambda_2 \leq 0$. Since $\lambda_1\lambda_2 > 0$ from (12), $\lambda_1 \leq \lambda_2 < 0$, and any positive value of $|L|$ satisfies the inequality (7). Therefore define $M_{Ru} \equiv \infty$ and $M_{Rl} \equiv 0$ (Figure 3(b)).
   c) If $D \geq 0$ and $\cos(\arg(L)) - |W_u||W_s| < 0$, then it follows from from (11) that $\lambda_1 + \lambda_2 > 0$. Since $\lambda_1\lambda_2 > 0$ from (12), $\lambda_2 \geq \lambda_1 > 0$, and $|L|$ satisfies inequality (7) when $|L| < \lambda_1$, or $|L| > \lambda_2$. Therefore define $M_{Ru} \equiv \lambda_1$ and $M_{Rl} \equiv \lambda_2$ (Figure 3(c)). Note that $M_{Ru} < M_{Rl}$ in this case.

2) Frequencies where $|W_u| < 1$ and $|W_s| > 1$. These are frequencies where there is relatively high confidence in the model, and disturbance attenuation is required.
Since $1 - |W_u|^2 > 0$ and $1 - |W_s|^2 < 0$,

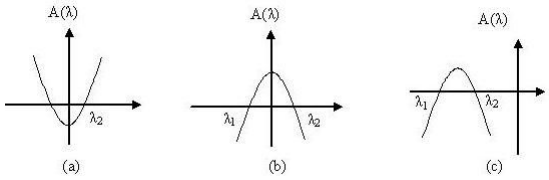

Fig. 4. Illustration of $A(\lambda)$ for different cases of $|W_u|$ and $|W_s|$.

the product of these terms contributes a positive value in the expression for D. Therefore $D \geq (\cos(\arg(L)) - |W_u||W_s|)^2 \geq 0$, and both λ_1 and λ_2 are real. Equation (12) implies that $\lambda_1\lambda_2 < 0$. This last fact implies that $\lambda_2 > 0$, and $\lambda_1 < 0$, and $|L|$ satisfies inequality (7) when $|L| > \lambda_2$. Therefore define $M_{Ru} \equiv \infty$ and $M_{Rl} \equiv \lambda_2$ (Figure 4(a)).

3) Frequencies where $|W_u| > 1$ and $|W_s| \leq 1$. These are frequencies where the magnitude of the modeling uncertainty is greater than the magnitude of the nominal model (there is relatively low confidence in the model), but disturbance attenuation is not required.
Since $1 - |W_u|^2 < 0$ and $1 - |W_s|^2 \geq 0$, the product of these terms contributes a nonnegative value in the expression for D. Therefore $D \geq (\cos(\arg(L)) - |W_u||W_s|)^2 \geq 0$, and both λ_1 and λ_2 are real. Equation (12) implies that $\lambda_1\lambda_2 < 0$. This last fact implies that $\lambda_1 > 0$ and $\lambda_2 < 0$, and $|L|$ satisfies inequality (7) when $0 < |L| < \lambda_1$. Therefore define $M_{Ru} \equiv \lambda_1$ and $M_{Rl} \equiv 0$ (Figure 4(b)),

4) Frequencies where $|W_u| > 1$ and $|W_s| \geq 1$. These are frequencies where there is low confidence in the model, but disturbance attenuation is required (Figure 4(c)).
Since $D = (\cos(\arg(L) - |W_u W_s|)^2 - (1 - |W_u|^2)(1 - |W_s|^2) = (|W_u| - |W_s|\cos(\arg(L))^2 + (|W_s|^2 - 1)(1 - \cos^2(\arg(L))$, where both terms on the right are nonnegative, $D \geq 0$ always holds. Both λ_1 and λ_2 are real. Equations (11) and (12) imply that $\lambda_1\lambda_2 > 0$ and $\lambda_1 + \lambda_2 < 0$, and thus $\lambda_2 \leq \lambda_1 < 0$. There is no positive value of $|L|$ satisfying inequality (7). Therefore M_{Ru} and M_{Rl} are undefined.
An important implication of this case that there is no compensator design that can achieve robust performance if there is requirement for disturbance rejection at frequencies where the magnitude of the

modeling uncertainty is greater than the magnitude of the model itself.

5) Frequencies where $|W_u| = 1$. These are frequencies where the lead coefficient of equation (8) is zero, and the inequality becomes linear.

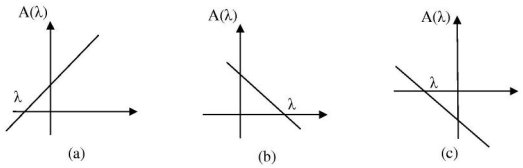

Fig. 5. Illustrations of $A(\lambda)$ for the three cases when $|W_u| = 1$.

a) If $|W_s| \leq 1$ and $\cos(\arg(L)) - |W_s| \geq 0$, then $\lambda < 0$ and any positive value of $|L|$ satisfies the inequality (7). Therefore define $M_{Ru} = \infty$ and $M_{Rl} = 0$ (Figure 5(a)).
b) If $|W_s| \leq 1$ and $\cos(\arg(L)) - |W_s| < 0$, then $\lambda > 0$, and any positive value of $|L| < \lambda$ satisfies the inequality (7). Therefore define $M_{Ru} = \lambda$ and $M_{Rl} = 0$ (Figure 5(b)).
c) If $|W_s| > 1$ then $\cos(\arg(L)) - |W_s| < 0$, then no positive value of $|L|$ satisfies inequality (7). Therefore M_{Ru} and M_{Rl} are undefined (Figure 5(c)).

Plotting M_{Ru} and M_{Rl} on the same axes as the open-loop Bode magnitude plot generates the RBode magnitude plot. Note that M_{Ru} and M_{Rl} are functions only of $\arg(L)$ and of the two weighting functions. Thus, multiplying $C(s)$ by a positive constant moves $|L|$ up or down on the magnitude plot, but does not alter the magnitude boundary functions. Any intersection between $|L|$ and M_{Ru} or M_{Rl} indicates that $|L|$ *does not* satisfy inequality (7).

III. APPLICATION

This section demonstrates how to use the RBode plots in the loop shaping process to synthesize a robust controller.

A. Active Tape Steering System

Tape drives are subject to lateral tape motion (LTM) caused by tape stacking imperfections and eccentricity of the supply reel (Figure 6). LTM causes damage to the tape edges when the tape strikes flanges on the guides or on the reels themselves. LTM has become a limiting factor in the development of high density, high performance tape drives. Researchers at Imation and Carnegie Mellon University have proposed to actively steer the tape by tilting one or more tape guides on the tape transport path to compensate for LTM. The designed active steering tape drive test stand is shown in Figure 7.

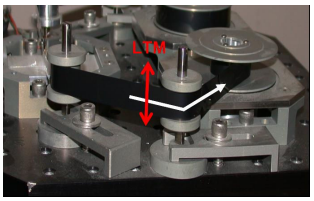

Fig. 6. Lateral Tape Motion(LTM) during tape transport.

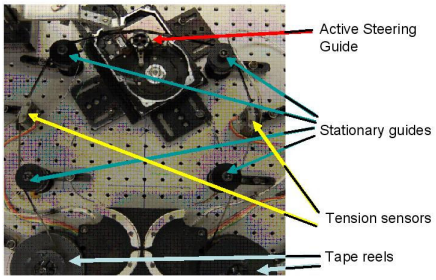

Fig. 7. The integrated hardware with second generation actuator and modified tape path.

B. Performance Specification

Significant disturbances in various frequency ranges are observed in open-loop LTM data collected during operation of the MTS tape transport. Dominant disturbances originate from either tape edge imperfections or tape drive reel imperfections. Disturbances below 25 Hz are of major concern and the specifications for the closed-loop system are

1) Zero steady state error for a constant disturbance;
2) Disturbance attenuation below 36 Hz (226 rad/sec);
3) At least 6 dB of attenuation for disturbances at frequencies below 16 Hz (100 rad/sec);
4) No more than 7 dB of disturbance amplification at any frequency;

The performance weighting function for the controller synthesis is:

$$W_s(\omega) = 0.45 \left(\frac{\omega^2 + 2.22e5}{\omega^2 + 1600} \right)^{1/2} \tag{13}$$

Figure 8 shows the magnitude response of W_s and its reciprocal, which is the desired upper bound for the sensitivity function. Note that this weighting function is not a transfer function.

C. Extraction of Plant Nominal Model and Uncertainties

A SigLab VNA dynamic signal analyzer was used to extract the characteristics of the integrated active steering tape transport system. Figure 9(a) shows the eight sets of experimental frequency response data collected at the operating conditions velocity = 4 m/s and tension = 1 N. The second order model

$$P_m = \frac{7.0e4}{s^2 + 593s + 4.4e4} \tag{14}$$

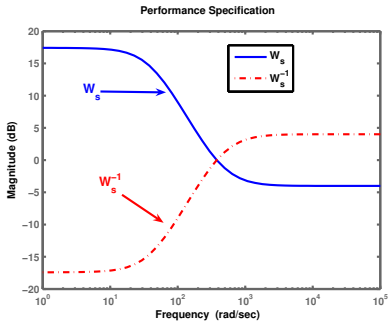

Fig. 8. Weighting function for robust performance.

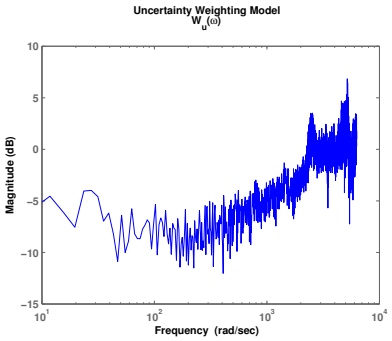

Fig. 10. The uncertainty weighting frequency response data model.

captures the most dominant system dynamics as indicated by the black solid curve in Figure 9(a). The transfer function P_m is used as the nominal system model.

The mismatch between the nominal model and the actual frequency response data in Figure 9(a) is treated as system uncertainties. The multiplicative mismatch between each frequency response data model and the nominal model is

$$\Delta_i = \frac{P_{collected\_i}}{P_m} - 1 \tag{15}$$

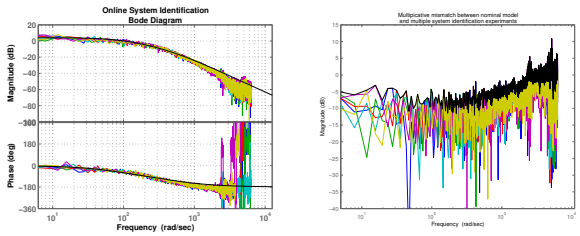

(a) (b)

Fig. 9. (a)Bode Diagram of the System Characteristics from online System Identification. (b)Bode Diagram of the Multiplicative differences.

In traditional robust controller design such as H_∞-synthesis, system uncertainty weighting function has to be represented as a stable transfer function. There is no such requirement for generating of the RBode plot. Instead of trying to fit a transfer function to the mismatches in Figure 9(b) to a transfer function, we simply constructed a tentative uncertainty weighting function as another frequency response data model which represents the worst-case model mismatch observed during system identification process, that is,

$$|\Delta_{max}(\omega)| = Max_{i=1,\cdots 8}|\Delta_i(j\omega)|, \forall\ \omega \tag{16}$$

The magnitude of $\Delta_{max}(\omega)$ is shown as the black envelope in Figure 9(b). The maximal mismatch model, however, includes not only the real plant model variations but also perturbations on plant input and output collected during the online system identification process, which shows up as several magnitude spikes at random frequency points. Figure 10 shows multiplicative uncertainty weighting function $Wu(\omega)$ used for the design, which is $|\Delta_{max}(\omega)|$ after outlier removal.

D. Loop shaping design using RBode plots

Figure 11(a) shows the RBode plot of the plant with PI compensator $C_{PI}(s) = 3.16\frac{s+100}{s}$. The compensated system violates the robust performance criterion between 200 rad/sec and 900 rad/sec approximately. The violations of the forbidden regions shown on the phase contours suggest using a lead compensator to shift the loop phase out of the forbidden region. Applying an 80 degree complex lead compensator at 1000 rads/s with 5 dB gain and damping ratio 0.96 $C_{clead}(s) = 7.67\frac{s^2+916s+2.3e5}{s^2+4e3s+4.3e6}$ results in Figure 11(b).

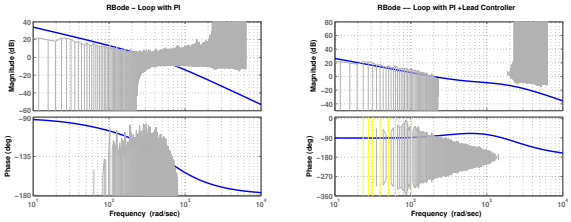

(a) (b)

Fig. 11. (a) RBode plot of the loop with a PI controller. (b) RBode plot of the loop with PI and complex lead compensator.

Now the RBode plot indicates a robustness violation between 20 rad/sec and 240 rad/sec. A 5.6dB gain does not change the boundary founctions of the RBode plot and lifts the loop magnitude into forbidden region. Figure 12 shows the RBode plot of the final loop.

The final controller used in the implementation is

$$C(s) = 46.2\frac{(s+100)(s^2+916s+2.3e5)}{s(s^2+4.0e3s+4.3e6)} \tag{17}$$

Note that the order of the controller is lower than what would have been obtained from an H_∞ synthesis. The controller order in H_∞ is equal to the order of the augmented plant. In this case the performance weighting function would have been at least first order. Likewise, the uncertainty weighting function would have been first order, and possibly much higher to get a tight bound on the modeling mismatch.

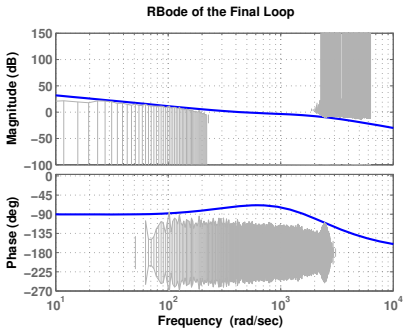

Fig. 12. RBode plot of the final loop.

Figure 13(a) shows the magnitude of $|W_s S + W_u T|$ with respect to frequency on a log-log plot. The magnitude is below unity for all frequencies, verifying that the design satisfies the robust performance criterion. As another check, Figure 13(b) shows the sensitivity functions of the controlled loop are below the desired upper bound W_s^{-1}. The sensitivity functions are frequency response data models calculated directly from the eight collected frequency response data models and the frequency response of the 3rd order controller converted from the transfer function.

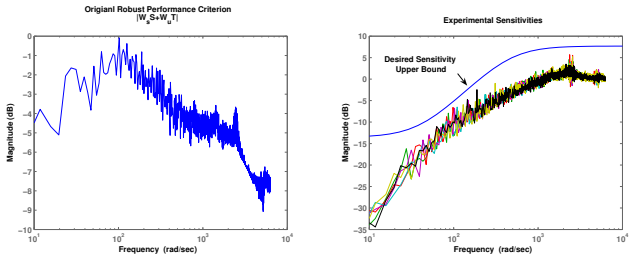

(a) (b)

Fig. 13. (a) Magnitude of the original robust performance criterion. (b) Sensitivity functions corresponding to the eight FRD models compensated by the controller of (17).

E. Simulation

A Simlink model was used to simulate the disturbance rejection performance of the nominal closed-loop system (Figure 14). The Simulink model injected LTM data collected during open-loop operation as an output disturbance. Figure 15 shows the simulation results of the nominal loop when the reference signal is zero. The simulation shows a reduction of the LTM by approximately 70%.

IV. CONCLUSION

This paper presented an improved version of the RBode plot where the robust performance criterion is explicitly represented as allowable and forbidden regions on the conventional Bode plot. The paper also presented a new derivation of the RBode plot that more clearly shows the relationship between the robust performance criterion and

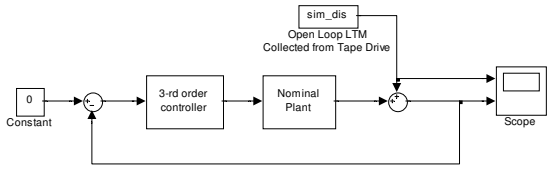

Fig. 14. Simulink model to simulate the nominal loop's performance.

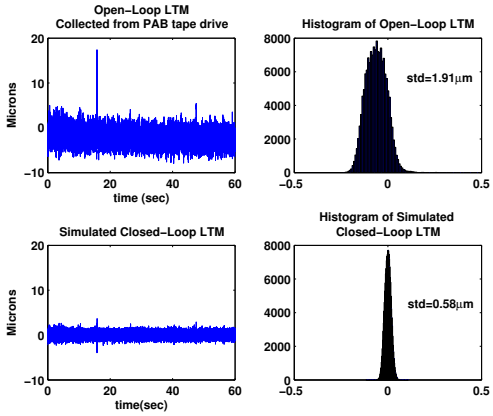

Fig. 15. Simulation results of the nominal loop.

the boundary functions of the forbidden regions with the aid of several graphs. An important feature of the RBode plot is the weighting functions do not need to be transfer functions.

The design example showed how to use the RBode plot for designing a controller with loop shaping to achieve robust performance. Significantly the uncertainty weighting function was obtained directly from experimental frequency response data rather than being the magnitude response of a transfer function. The resulting design had lower order than what would have been obtained from an automated synthesis method without order reduction.

REFERENCES

[1] G.J. Balas, J. Doyle, K. Glover, A. Packard, and R.Smith, μ-Analysis and Synthesis Toolbox User's guide. The Mathworks Inc., Second Edition, 1995.

[2] D. McFarlane and K. Glover, A loop shaping design procedure using H_∞ synthesis, *IEEE Transactions on Automatic Control*, 37(6),1992.

[3] L. Xia and W. Messner, Loop shaping for robust performance using the RBode plot, *Proceedings of the 2005 American Controls Conference*, Portland, OR, June 2005, p. 2869-74.

[4] J. Doyle, B. Francis and A. Tannenbaum, *Feedback Control Theory*. Macmillan Publishing Company, 1992.

[5] W. Messner, Some advances in loop shaping with applications to disk drives, *Proceedings of the 2002 American Control Conference*, 37(2), 2001.

[6] S.C. Smith and W. Messner, Loop shaping with closed-loop magnitude contours on the Bode plot, *Proceedings of the 2002 American Controls Conference*, Anchorage, AK, May 2002, p 2747-52.